INTERNATIONAL JOURNAL FOR NUMERICAL METHODS IN FLUIDS
Int. J. Numer. Meth. Fluids 2007; **53**:1221–1242
Published online 28 December 2005 in Wiley InterScience (www.interscience.wiley.com). DOI: 10.1002/fld.1162

A modified space–time finite element method for simulation of immiscible incompressible two-phase flow in heterogeneous porous media

P. A. Ferdowsi[‡] and Mehrdad T. Manzari[*,†]

School of Mechanical Engineering, Sharif University of Technology, Tehran 11365-3567, Iran

SUMMARY

In this paper, a modified space–time method is presented for the simulation of convection–diffusion equations. The new method differs from the original space–time method in the sense that the weight functions for space and time are different. The performance of the proposed algorithm is studied for numerical simulation of incompressible immiscible two-phase flow in porous media. The governing equations consist of one conservation of mass equation for each phase, the Darcy law and one capillary-saturation correlation for the flow. By defining a global pressure, the governing equations lead to a system of nonlinear equations in terms of this global pressure, the velocity components and the saturation of one phase. The flow equations are solved for the global pressure and velocity components using a stabilized mixed finite element method while the saturation equation is solved by the standard and modified space–time element methods. The performance of the proposed space–time method is compared with that of the original Petrov–Galerkin space–time method for both linear and nonlinear cases. The effect of the tuning parameters of the standard method, grid size and the capillary pressure are studied for a one-dimensional problem. A stability analysis is also carried out for the proposed space–time method. Finally, to demonstrate the capability of the proposed method in dealing with homogeneous and heterogeneous problems two-dimensional water-flooding five-spot test cases are studied. Copyright © 2005 John Wiley & Sons, Ltd.

KEY WORDS: space–time element; porous media; immiscible; incompressible; two-phase; heterogeneous

1. INTRODUCTION

The numerical study of multi-phase flow in porous media has been a major challenge for the scientific community. This manifests itself when dealing with realistic engineering problems

*Correspondence to: Mehrdad T. Manzari, School of Mechanical Engineering, Sharif University of Technology, Tehran 11365-3567, Iran.
†E-mail: mtmanzari@sharif.edu
‡E-mail: p_ferdowsi@mehr.sharif.edu, p.ferdowsi@gmail.com

Contract/grant sponsor: Center of Excellence in Energy Conversion

Received 15 August 2005
Revised 14 November 2005
Accepted 15 November 2005

where the accuracy and computational efficiency requirements are to be met. One application which has attracted significant attention is the fluid flow in hydrocarbon reservoirs. The main challenge for today's reservoir engineers is how to enhance the rate of production so that it remains economically viable. Such methods are known as enhanced oil recovery (EOR) methods. Various EOR technologies have been introduced in the literature [1–5]. It is known that the rate of production from a hydrocarbon reservoir decreases during its production lifetime as a result of excessive pressure drop in the reservoir. In order to sustain the rate of production, it is necessary to maintain the reservoir pressure. Water flooding is one of the recovery methods in which pressurized water is injected from water wells into the reservoir to displace the resident oil towards the low-pressure production wells. Enhanced oil recovery processes have all characteristics of multi-phase flow in a porous medium and prediction of its performance is of significant practical importance. This prediction can be achieved by mathematical modelling and using numerical tools [2, 4, 6, 7].

For the sake of simplicity, only immiscible incompressible flow of oil and water phases is considered in the present work. Here, the effect of temperature variations on the phase and physical properties of the formation are ignored. The governing equations include the generalized Darcy's law and the continuity equations for each phase, which are highly coupled. In addition, two constitutional relations are required for the relative permeability of phases and the capillary pressure between the two phases in order to close the system of equations. The governing equations can be described in terms of various choices of the dependent variables [7]. One popular choice uses the concept of a *global pressure*, which takes an intermediate value between the pressures of two phases [6, 8, 9]. A major advantage of this approach is that it produces models of known mathematical nature for which rigorous mathematical and numerical treatments exist.

There are various solution strategies for handling the above mentioned equations which are normally time dependent. This ranges from a fully explicit to a fully implicit approach. A widely accepted approach for this purpose is the so-called IMplicit in Pressure and Explicit in Saturation (IMPES) algorithm [6, 7]. This approach facilitates sequential solution of the pressure and saturation equations. In other words, as the pressure varies only slightly in time, at each time step the global pressure and velocity equations are first solved implicitly. Subsequently, the saturation equation is solved explicitly to complete one time step.

The finite element method has been widely used for conservation laws and flow problems [10–12]. The method has been particularly successful in the field of reservoir simulation [6, 7, 10, 13–16]. When IMPES algorithm is used, the velocity field explicitly appears in the saturation equation. Therefore, the accuracy of velocity field becomes a vital factor to achieve accurate saturation distributions. In addition, since the satisfaction of the conservation of mass is critical in the reservoir engineering simulations, the flow equations are frequently solved using the mixed finite element method [13, 15–17]. The major drawback of the mixed methods is their complexity as different interpolation functions are required for the velocity and pressure variables to satisfy the so-called inf–sup condition [11, 15, 17]. Masud and Hughes [15] introduced a stabilized mixed finite element (SMFE) method, which requires no mesh-dependent parameter and satisfies both local and global mass conservation. Their method also has an improved convergence rate in comparison with other mixed finite element methods.

The saturation equation is a transient convective-dominant equation, which requires particularly a time accurate and computationally efficient method. There are a number of numerical schemes which can be used for this purpose. Most of such methods introduce some

numerical diffusion to suppress the spurious numerical oscillations. One choice involves using the Petrov–Galerkin method for spatial discretization along with the so-called θ-method for temporal discretization [17, 18]. Also, Espedal and Ewing developed a family of preconditioned characteristic Petrov–Galerkin subdomain methods for two-phase immiscible flows that suits parallel computing [19]. Helmig [7] proposed a modified Petrov–Galerkin method for the solution of the saturation equation, which alleviates the spurious numerical oscillations induced due to the presence of the dominant convective term. In this method, the order of weight functions is higher than the basis functions by a factor of two. Cardle [20] proposed a similar explicit method for solving advection–diffusion problems in which the weight functions used for the time derivative differ from those used for the spatial derivatives.

A family of finite element method which has attracted the attention of researchers is the so-called space–time element method (STEM). An excellent presentation of these methods was given by Yu and Heinrich [21, 22] and Pepper and Heinrich [18]. In this work, the Petrov–Galerkin space–time element method is considered. The method introduces some numerical diffusion and dispersion, which are dependent on two tuning parameters. When solving linear equations, the method is at least second-order accurate in space and an optimum value can be found for each of these parameters by a truncation analysis [18, 21, 22]. The method has been also extended to the solution of nonlinear equations [23].

This paper presents an algorithm for solving the flow of two immiscible incompressible fluids in a heterogeneous porous formation. First, a detail study of the problem in one dimension is given where the pressure and velocity equations are solved using the SMFE method. The saturation equation is solved using two versions of the space–time element method; the Standard STEM (SSTEM) and the Modified STEM (MSTEM) methods. The performance of the two methods is compared and the effect of the capillary pressure and the tuning parameters of the SSTEM are investigated using three 1D test cases. In the first case, it is assumed that the phase relative permeability is linear, hence, becoming a linear pure advection problem. In the second case, the nonlinear model of Brooks–Corey for the phase relative permeability is considered. In the third case, the effect of capillary pressure is included and a nonlinear advection–diffusion problem is solved. A stability analysis of the modified method (MSTEM) is also presented. The algorithm is then extended to the 2D cases. For 2D problems, again, the pressure and velocity equations are solved by the SMFE method. However, due to superior performance shown by the MSTEM, only this method is employed for solving the saturation equation in 2D. Three five-spot problems including homogeneous and heterogeneous media are solved and the effect of element size is investigated.

2. MATHEMATICAL FORMULATION

2.1. Mathematical model

The governing equations for the physical phenomenon of interest in this work are those of general multi-phase flow in a porous media. These consist of the conversation of mass and momentum equations which are elaborated below.

Conservation of mass. The mass balance equation for each phase is given by

$$\frac{\partial}{\partial t}(\varepsilon S_i B_i) + \nabla \cdot \mathbf{q}_i = 0 \tag{1}$$

where subscript i refers to ith phase, t is time, ρ is density, $\mathbf{q}$ is the volumetric flow rate vector, ε is the formation porosity. Also, $B_i = \rho_i/\rho_{i,\mathrm{ref}}$ is the volume factor where ρ_{ref} represents the density at a given reference condition. This quantity is unity for the incompressible case studied here. In Equation (1), the saturation S_i is defined as the ratio of the volume of pores filled with phase i to the volume of the pore space. It is noted that $\sum_i S_i = 1$.

Conservation of momentum. The generalized Darcy's law for the ith phase, is written as

$$\mathbf{q}_i = -d_i k_{ri} \boldsymbol{K} \cdot \boldsymbol{\nabla}(p_i - \rho_i g z) \tag{2}$$

where $d_i = B_i/\mu_i$ is the mobility factor, k_{ri} is the relative permeability, p_i is the pressure of the ith phase and $\boldsymbol{K}$ is the tensor of absolute permeability. The gravitational acceleration is g and z is the component of the position vector in the direction of the gravitational field. In this study a two fluid system consisting of water and oil is considered.

The unknowns in the above equations are the pressure, volumetric flow rate and saturation of phases. To have a complete set of equations, these should be accompanied by appropriate constitutive relations for the capillary pressure and relative permeability.

As mentioned before, to reach a mathematically identifiable model, the global pressure concept is used [6, 8, 9]. This is defined as

$$P = \frac{1}{2}(P_{\mathrm{w}} + P_{\mathrm{o}}) + P_{\mathrm{CM}}(x) \int_{S_{\mathrm{C}}}^{S_{\mathrm{w}}} \left(\upsilon_{\mathrm{w}}(S) - \frac{1}{2}\right) \frac{\mathrm{d}\, p_{\mathrm{C}}(S)}{\mathrm{d}S}\, \mathrm{d}S \tag{3}$$

where $\upsilon_i = d_i k_i/d$ is the ith phase fractional flow and $d = \sum_i d_i k_{ri}$ is the global mobility. This is in fact an integral transform of the original equations whose role is to weaken the decoupling among the equations. In general, it is assumed that the effect of the capillary pressure contains two parts; one is dependent on the position and the other is dependent on saturation. In other words, it is assumed that $P_{\mathrm{C}}(\mathbf{x}, S) = P_{\mathrm{CM}}(\mathbf{x}) p_{\mathrm{C}}(S)$. The capillary pressure vanishes at S_{C}. By using the global pressure definition and after some mathematical manipulations and also assuming that the fluids are immiscible incompressible, the following equations are obtained [6, 8, 9]:

$$\mathbf{q} = -\,\mathrm{d}\boldsymbol{K} \cdot \left[\boldsymbol{\nabla} P + \boldsymbol{\nabla} P_{\mathrm{CM}}(x) \int_{S_{\mathrm{C}}}^{S_{\mathrm{w}}} \frac{\mathrm{d}\upsilon_{\mathrm{w}}(S)}{\mathrm{d}S} p_{\mathrm{C}}(S)\, \mathrm{d}S - \upsilon_{\mathrm{o}}\upsilon_{\mathrm{w}}\, \mathrm{d}\boldsymbol{K} \cdot \boldsymbol{\nabla}((\rho_{\mathrm{w}} - \rho_{\mathrm{o}}) g z)\right] \tag{4}$$

$$\boldsymbol{\nabla} \cdot \mathbf{q} = 0 \tag{5}$$

$$\varepsilon \frac{\partial S_{\mathrm{w}}}{\partial t} + \frac{\mathrm{d}\upsilon_{\mathrm{w}}}{\mathrm{d}S_{\mathrm{w}}} \mathbf{q} \cdot \boldsymbol{\nabla} S_{\mathrm{w}} - \boldsymbol{\nabla} \cdot \left[\upsilon_{\mathrm{o}}\upsilon_{\mathrm{w}} P_{\mathrm{CM}} \frac{\mathrm{d}\, p_{\mathrm{C}}}{\mathrm{d}S_{\mathrm{w}}}\, \mathrm{d}\boldsymbol{K} \cdot \boldsymbol{\nabla} S_{\mathrm{w}} - \upsilon_{\mathrm{o}}\upsilon_{\mathrm{w}}\, \mathrm{d}\boldsymbol{K} \cdot \boldsymbol{\nabla}((\rho_{\mathrm{w}} - \rho_{\mathrm{o}}) g z)\right] = 0 \tag{6}$$

Equations (4) and (5) describe the velocity and pressure fields and Equation (6) gives the water saturation distribution. In the present work, the effect of gravitational force is neglected. Therefore, the final set of equations becomes

$$\mathbf{q} = -\,\mathrm{d}\boldsymbol{K} \cdot \left[\boldsymbol{\nabla} P + \boldsymbol{\nabla} P_{\mathrm{CM}}(x) \int_{S_{\mathrm{C}}}^{S_{\mathrm{w}}} \frac{\mathrm{d}\upsilon_{\mathrm{w}}(S)}{\mathrm{d}S} p_{\mathrm{C}}(S)\, \mathrm{d}S\right] \tag{7}$$

$$\boldsymbol{\nabla} \cdot \mathbf{q} = 0 \tag{8}$$

$$\varepsilon \frac{\partial S_{\mathrm{w}}}{\partial t} + \frac{\mathrm{d}\upsilon_{\mathrm{w}}}{\mathrm{d}S_{\mathrm{w}}} \mathbf{q} \cdot \boldsymbol{\nabla} S_{\mathrm{w}} - \boldsymbol{\nabla} \cdot \left[\upsilon_{\mathrm{o}}\upsilon_{\mathrm{w}} P_{\mathrm{CM}}(x) \frac{\mathrm{d}\, p_{\mathrm{C}}}{\mathrm{d}S_{\mathrm{w}}}\, \mathrm{d}\boldsymbol{K} \cdot \boldsymbol{\nabla} S_{\mathrm{w}}\right] = 0 \tag{9}$$

It is also assumed that $P_{CM}(\mathbf{x}) = 1$. If the effect of the capillary pressure is negligible then the following set of equations is yielded [7]:

$$\mathbf{q} = -\,\mathrm{d}\boldsymbol{K} \cdot \boldsymbol{\nabla} P \tag{10}$$

$$\boldsymbol{\nabla} \cdot \mathbf{q} = 0 \tag{11}$$

$$\varepsilon \frac{\partial S_{\mathrm{w}}}{\partial t} + \frac{\mathrm{d}\upsilon_{\mathrm{w}}}{\mathrm{d}S_{\mathrm{w}}} \mathbf{q} \cdot \boldsymbol{\nabla} S_{\mathrm{w}} = 0 \tag{12}$$

Equation (12) is the so-called Buckley–Leverett equation, which is a pure convection equation, and it is known that some difficulties arise in its numerical simulations.

2.2. *Boundary conditions*

In order to have a unique solution for the aforementioned system of equations, a proper set of boundary conditions is required. Here, for the global pressure equations, the boundary of domain is decomposed into disjoint open sets Γ_{pD} and Γ_{pN} corresponding to Dirichlet ($p = p_{\mathrm{D}}$) and Neumann ($\mathbf{q} \cdot \mathbf{n} = q_{\mathrm{inj}}$) boundary conditions. Similarly, Γ_{sD} and Γ_{sN} are the Dirichlet and Neumann boundary regions for the saturation equation, respectively. The Dirichlet boundary conditions are applied on the injection and production well(s) while the Neumann boundary conditions are applied on the regions where no-flow boundary exists.

3. DISCRETIZATION AND NUMERICAL METHODS

Referring to the governing equations obtained for the flow field, e.g. (7) and (8), it is observed that the velocity variable is strongly dependent on the gradient of pressure. One way to solve these equations is to derive a Poisson for the pressure by combining them and after solving this Poisson equation, obtain the velocity field by taking the gradient of the pressure field. It is known, however, that this approach will introduce significant numerical error in the solution. A better approach can be devised by employing the so-called mixed finite element method in which both variables are calculated simultaneously. In this way, $\mathbf{q}$ is computed directly and coupling among equations is preserved. It should be noted that in 1D cases it is not required to solve the global pressure equation and by knowing the rate of injection or production, the volumetric flow is directly specified. Details of the discretization of (10) and (11) using a mixed method can be found elsewhere [6, 13, 15, 16]. In this work the SMFE is used for the solution of these equations [15]. The SMFE method satisfies both local and global conservation properties, which are important in reservoir simulation. Besides, the rate of convergence of this scheme is better than the conventional mixed methods [15].

The water saturation equation, (9), is discretized by the space–time element method (STEM). Since in this method the shape functions differ from weight functions, STEM belongs to the category of the Petrov–Galerkin method [18, 22]. This method improves the accuracy of the numerical scheme by introducing balancing diffusion and dispersion terms. Generally,

the weight functions in the STEM can be written in the following form:

$$W_i = M_i + \frac{h}{2\|\mathbf{V}\|}\left(\alpha + \frac{\beta \Delta t}{2}\frac{\partial}{\partial t}\right)\mathbf{V}\cdot\nabla M_i \tag{13}$$

where M_is refer to the test functions constructed using an even quadratic function in time and linear in space, h is the element length in the flow direction, $\mathbf{V}$ is the flow velocity, and α and β are tuning parameters. The tuning parameters are determined from the truncation error and stability analysis as [18, 22]:

$$\alpha = \coth\left(\frac{\gamma}{2}\right) - \frac{2}{\gamma} \tag{14}$$

$$\beta = \frac{C}{3} - \frac{2\alpha}{\gamma C} \tag{15}$$

with γ and C being the Peclet and Courant numbers, respectively. Using these parameters increases the accuracy of the scheme to third order in space and second order in time [18, 22]. For 1D problems, the test functions M_i are written as

$$\begin{aligned} M_1(\eta,\tau) &= \tfrac{1}{2}(1-\eta)(1-\tau^2) \\ M_2(\eta,\tau) &= \tfrac{1}{2}(1+\eta)(1-\tau^2) \end{aligned} \tag{16}$$

where η and τ represent space and time coordinates, respectively. A plot of function M_1 is shown in Figure 1 (left). Stability analysis for a linear convection–diffusion PDE employing

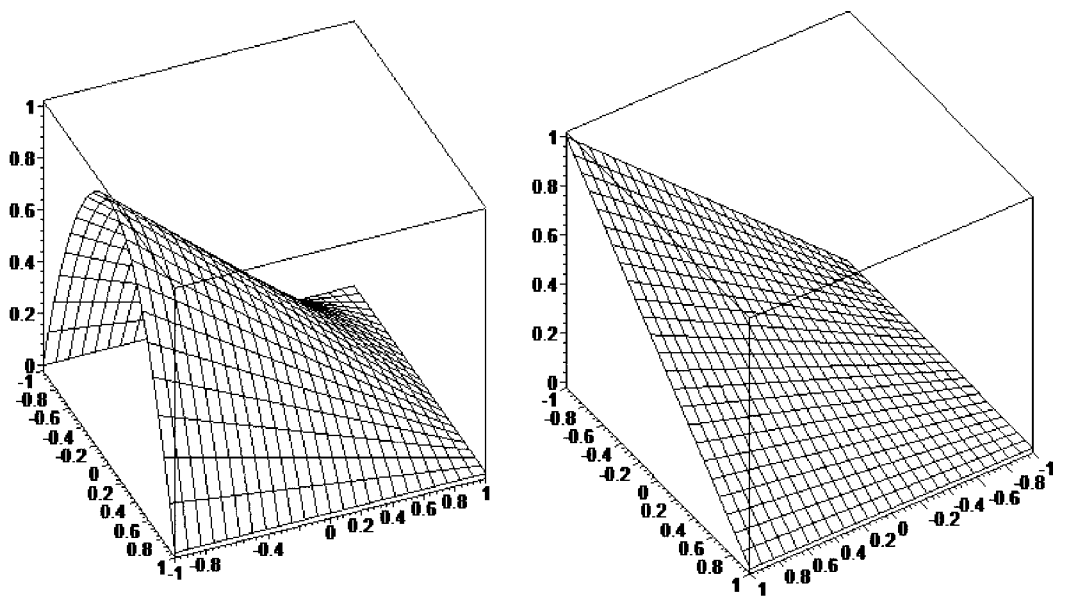

Figure 1. Test functions (M_1): (left) quadratic in time and linear in space and (right) bilinear in time and space.

test functions given in (16) shows that if β is zero then the algorithm is unconditionally stable but its spatial accuracy is reduced to the second order [22]. If both of the adjusting parameters set to their optimum values, then the algorithm will be stable only for $C \leqslant 1$ [18, 22]. It should be noted that the optimum values for the tuning parameters, α and β, are obtained from Equations (14) and (15) only if the test functions are quadratic in time. If the test functions are bilinear, then the optimum values of the tuning parameters are obtained from [22]

$$\alpha = \frac{6}{C\gamma}\left[\coth\left(\frac{\gamma}{2}\right) - \frac{2}{\gamma}\right] \tag{17}$$

$$\beta = \left(1 - \frac{6}{C\gamma}\right)\left[\coth\left(\frac{\gamma}{2}\right) - \frac{2}{\gamma}\right] \tag{18}$$

Yu and Heinrich [22] have shown that the use of weight functions which are bilinear in space and time results in an over-damped solution for all wave numbers while the quadratic weight functions do not show such a shortcoming [22]. In this paper, test functions are opted to be quadratic in time and linear in space. Figure 1 (left) shows a plot of such a test function.

In the rest of this section, two algorithms are presented based on the STEM for solving a convection–diffusion equation. In the first algorithm, Equation (9) is multiplied by a weight function. After using the integration by parts, the following equation is obtained:

$$\int_\Omega W_{ti}\varepsilon\frac{\partial S_\mathrm{w}}{\partial t}\,\mathrm{d}\Omega + \int_\Omega W_{si}\frac{\mathrm{d}\upsilon_\mathrm{w}}{\mathrm{d}S_\mathrm{w}}\mathbf{q}\cdot\boldsymbol{\nabla}S_\mathrm{w}\,\mathrm{d}\Omega + \int_\Omega \boldsymbol{\nabla}W_{si}\cdot\left[\upsilon_\mathrm{o}\upsilon_\mathrm{w}P_\mathrm{CM}\frac{\mathrm{d}p_\mathrm{C}}{\mathrm{d}S_\mathrm{w}}\,\mathrm{d}\boldsymbol{K}\cdot\boldsymbol{\nabla}S_\mathrm{w}\right]\mathrm{d}\Omega$$
$$= \int_\Gamma W_{si}\cdot\left[\upsilon_\mathrm{o}\upsilon_\mathrm{w}P_\mathrm{CM}\frac{\mathrm{d}p_\mathrm{C}}{\mathrm{d}S_\mathrm{w}}\,\mathrm{d}\boldsymbol{K}\cdot\boldsymbol{\nabla}S_\mathrm{w}\right]\mathrm{d}\Gamma \tag{19}$$

Here, the weight functions W_{ti}, applied to the time derivative can be different from the weight functions W_{si} applied to the spatial derivatives [20, 24].

1st Algorithm: In the first algorithm, the Standard STEM (SSTEM) approach is used. That is $W_{si} = W_{ti}$ which are obtained from Equation (13). Details can be found in References [18, 22].

2nd Algorithm: In the second algorithm, a Modified STEM (MSTEM) approach is used. The weight functions W_{si} are obtained from Equation (13) while the weight functions W_{ti} are the same as the test functions, given by Equation (16). It will be shown later that this choice significantly improves the accuracy of the solution.

3.1. Stability analysis

Applying these weight functions to the following 1D linear advection–diffusion equation:

$$\frac{\partial\phi}{\partial t} + u\cdot\frac{\partial\phi}{\partial x} - D\frac{\partial^2\phi}{\partial x^2} = 0 \tag{20}$$

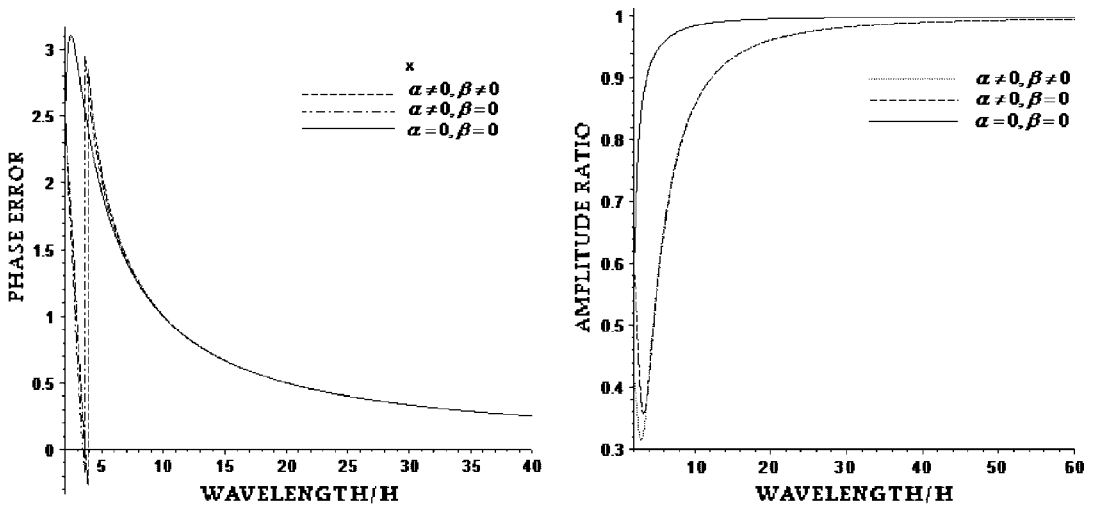

Figure 2. Phase error (left) and damping factor (right) of the modified algorithm.

results in the following difference equation for the jth node:

$$\frac{1}{9}[(\phi_{j-1}^{n+1}-\phi_{j-1}^{n})+4(\phi_{j}^{n+1}-\phi_{j}^{n})+(\phi_{j+1}^{n+1}-\phi_{j+1}^{n})]$$
$$+\frac{C}{6}[(\phi_{j+1}^{n+1}+\phi_{j+1}^{n})-(\phi_{j-1}^{n+1}+\phi_{j-1}^{n})]-\left[\frac{C}{6}(\alpha-\beta)+\frac{C}{3\gamma}\right](\phi_{j+1}^{n+1}-2\phi_{j}^{n+1}+\phi_{j-1}^{n+1})$$
$$-\left[\frac{C}{6}(\alpha+\beta)+\frac{C}{3\gamma}\right](\phi_{j+1}^{n}-2\phi_{j}^{n}+\phi_{j-1}^{n})=0 \tag{21}$$

where $C=u\Delta t/\Delta x$ is the Courant number and $\gamma=u\Delta x/D$ is the Peclet number. Inserting $\phi_j^n=\xi^n e^{ikjh}$ in Equation (21), using Euler's formula ($e^{i\alpha}=\cos\alpha+i\sin\alpha$) and letting $\theta=kh$, the amplification factor ξ is obtained from:

$$\xi=\frac{\left[\frac{2}{9}\left(1+2\cos^2\frac{\theta}{2}\right)-\frac{2C}{3}\left(\alpha+\beta+\frac{2}{\gamma}\right)\sin^2\frac{\theta}{2}\right]-i\left(\frac{C}{3}\sin\theta\right)}{\left[\frac{2}{9}\left(1+2\cos^2\frac{\theta}{2}\right)+\frac{2C}{3}\left(\alpha-\beta+\frac{2}{\gamma}\right)\sin^2\frac{\theta}{2}\right]+i\left(\frac{C}{3}\sin\theta\right)} \tag{22}$$

This stability analysis shows that if $\beta=0$ the algorithm is unconditionally stable for all α. If $\beta\neq 0$, then $|\xi|<1$ only if $C\leqslant 1$, so the method becomes only conditionally stable. The damping factor and the phase error are shown in Figure 2 for $\gamma=20$ and $C=0.8$. It is seen that the method practically produces no phase error when the wave number is $L/h=5$ (L is the wave length) while it produces some damping for values smaller than $L/h=10$. It is also observed that the damping factor for MSTEM method is relatively larger than that of the standard method. A comparison of the results obtained using the modified algorithm with the

standard method reveals that both methods give identical phase errors provided that the same values are used for the tuning parameters. As it can be seen from Figure 2 and Equation (22), when employing identical values for the tuning parameters, the element size must be halved to achieve the same damping factor using the MSTEM. To find the optimum values of the tuning parameters of the modified algorithm a truncation error analysis is required.

3.2. Solution procedure

It must be emphasized that for 1D problems there is no need to solve the global pressure and total velocity equations. For 2D cases, however, the IMPES algorithm is used. The matrices are stored using the general storage scheme by rows or compressed sparse row (CSR) storage format [25]. The resulting linear system of equations is solved using a sparse version of the generalized minimum residual method (GMRES) [25]. For the system of flow equations, an ILU precondition is also used. The saturation equation is linearized using Picard's iterative technique at each time step. When the capillary pressure is nonzero, an under-relaxation parameter 0.5 is used while no under-relaxation is required when the capillary pressure is negligible.

4. TEST CASES

In this section, several test cases including 1D and 2D problems are studied. For 1D test cases, both zero and nonzero capillary pressure situations are studied using the SSTEM and MSTEM algorithms. The 2D test cases are solved using both the SSTEM and the MSTEM algorithms.

In the 1D problem, water is injected from one end and oil is produced from the other end. The filed is 300 m long and the production duration is 1500 days. The analytical solution for this problem with zero capillary pressure can be found in Reference [7]. For all calculations, the time step was one day. Dirichlet boundary conditions are applied for the saturation equation at the injection and production wells. The boundary conditions for the saturation variable are defined as follows:

$$\begin{aligned} S_w &= 1 - S_{rn} \quad \text{at injection well} \\ S_w &= S_{rw} \quad \text{at production well} \end{aligned} \tag{23}$$

where S_{rn} is the residual saturation of the nonwetting phase and S_{rw} is the residual saturation of the wetting phase.

The second test case involves a two-phase flow problem in a five-spot model. A schematic of the computational domain is a $300\,\text{m} \times 300\,\text{m}$ square and the wells are represented in the form of two quarter circles of 30 m radius taken out of it. The physical properties of both fluids are given in Table I. Three choices for the absolute permeability of the matrix are considered here; homogeneous, block heterogeneous and continuous heterogeneous. The rate of water injection is 0.12 kg/s. Helmig [7] has suggested that it is better to distribute the injection rate over the well's boundary using a uniform distribution normal to the boundary. The Dirichlet boundary conditions for the saturation equation are applied at the injection and production wells in the same way as for the 1D problem. The boundary conditions are

Table I. Fluid and matrix properties (1D).

Water density, ρ_w	$1000\,kg/m^3$
Oil density, ρ_o	$1000\,kg/m^3$
Water dynamics viscosity, μ_w	$0.001\,kg/ms$
Oil dynamics viscosity, μ_o	$0.001\,kg/ms$
Residual water saturation, S_{rw}	0 [—]
Residual oil saturation, S_{rn}	0 [—]
Oil production rate, q_o (in 1D case)	$1.5 \times 10^{-4}\,kg/m^2\,s$
Initial saturation	0 [—]
Capillary pressure model (in 1D case)	Brooks–Corey model $P_d = 1\,Pa$, $\lambda = 2$
Relative permeability model	Brooks–Corey model $\lambda = 2$
Absolute permeability, K	$10^{-7}\,m^2$
Porosity, ε	0.2 [—]

as follows:

$$\begin{aligned} &S_w = 1 - S_{rn}, \quad |\mathbf{q}| = 0.12\,kg/s && \text{injection well} \\ &S_w = S_{rw}, \quad P = 10^5\,Pa && \text{production well} \\ &\mathbf{q}\cdot\mathbf{n} = 0 && \text{rest of boundary} \end{aligned} \tag{24}$$

5. NUMERICAL RESULTS AND DISCUSSION

5.1. One-dimensional case I: linear relative permeability with zero capillary pressure

In this case, the saturation equation becomes a linear first-order partial differential equation. The linear pure convection problem has been extensively studied by Heinrich and Yu [22], Hughes [15], Helmig [7], Chavent and Jaffre [6], Cardle [20] and Huyakorn and Nilkuha [24]. The linear advection–diffusion problem has been studied by Heinrich and Pepper in Reference [18] using STEM. Figure 3 shows the computed saturation profiles after 500 and 1500 days using the SSTEM and MSTEM algorithms using optimum values of the tuning parameters, α and β.

Figure 4(a) shows the effect of tuning parameters of the standard method on the solution at 1500 days. It is clear that when no tuning parameter is used, the solutions exhibit oscillations. For this case, it is seen that the tuning parameter β does not play an important role. In fact, as the Courant number decreases, the numerical diffusion is also lowered and the numerical dispersion does not alter the position of the front. On the other hand, a lower Courant number decreases the numerical diffusion, hence, diminishes the effect of the parameter β.

As it is apparent from figures, the SSTEM algorithm captures the discontinuity well but some numerical oscillations appear at the wave front. The over-shoots and under-shoots in the numerical solution of the first algorithm could be removed by using the concept of difference or slope limiters [26, 27]. Lapidus has developed an artificial diffusion technique in which extra diffusion is added explicitly to the original equation [28]. The implementation of this method for nonlinear problems becomes difficult as the amount of diffusion is dependent on

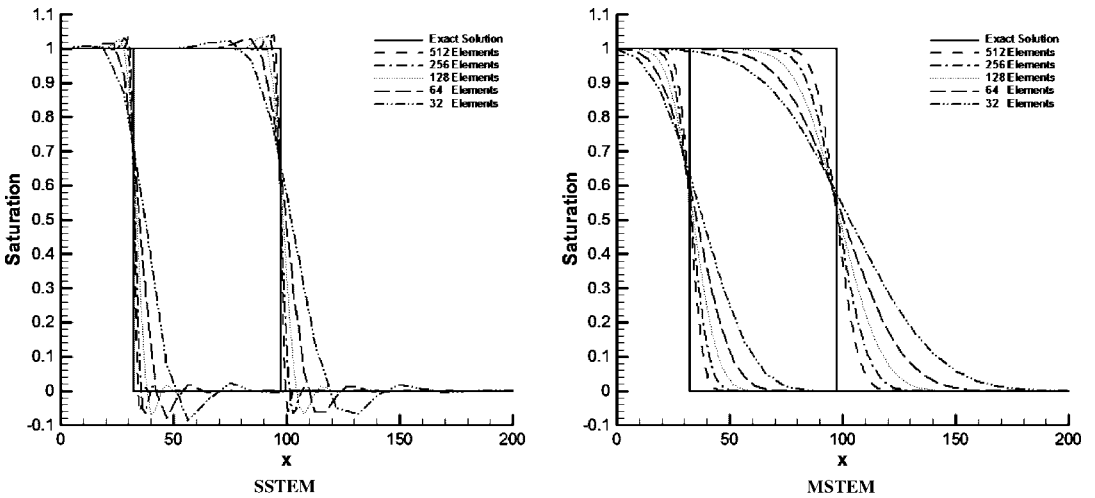

Figure 3. Case I—comparison of results obtained on various grids using SSTEM and MSTEM algorithms with the exact solution.

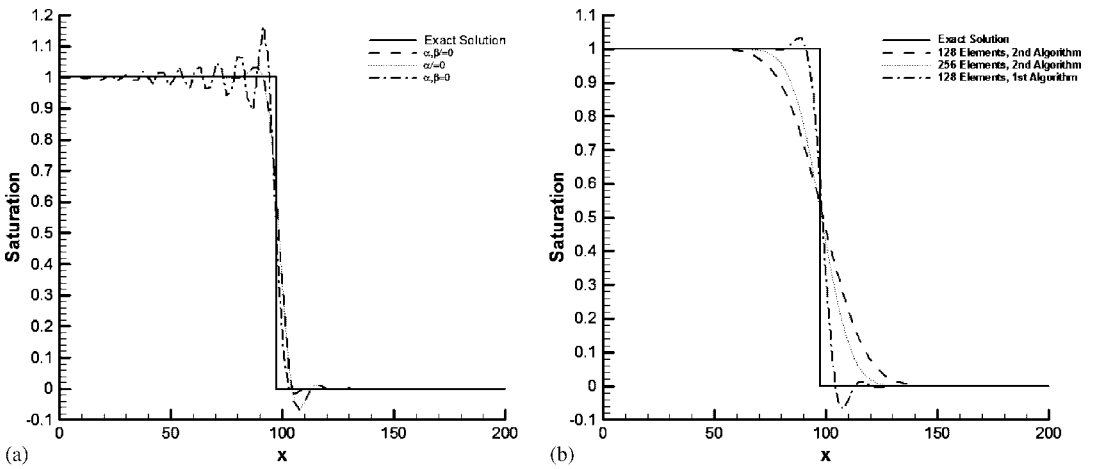

Figure 4. Case I—(a) effect of tuning parameters on solution of the using SSTEM algorithm using 128 elements; and (b) comparison of results obtained by SSTEM and MSTEM algorithms.

the time step, grid size, and the velocity field. On the other hand, the MSTEM algorithm has not captured the front as sharp as the SSTEM but gives a monotonic solution. Figure 4(b) compares these two solutions. As it was mentioned before, when using MSTEM, halving the grid size produces solutions as sharp as those of SSTEM but without any over-shoots or under-shoots.

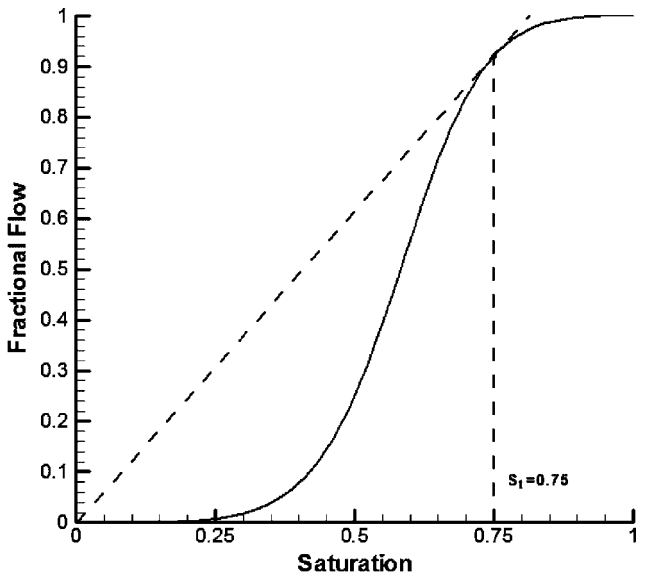

Figure 5. Fractional flow diagram and corresponding tangential saturation for zero residual saturation.

5.2. One-dimensional case II: Brooks–Corey model for relative permeability with zero capillary pressure

For this case an analytical solution can be found in Reference [7]. According to this reference the saturation of the wave front must remain constant and equal to the saturation of the tangential point on the fractional flow diagram shown in Figure 5. In this article, the residual saturation is assumed to be zero, and therefore the saturation of the tangential point is 0.75. As the saturation of the wave front is constant and also its velocity does not alter, after 1500 days the position of the wave front must be at $x = 119.29$. The numerical solution of this case using the SSTEM algorithm with optimum values for the tuning parameters is shown in Figure 6(a). The effect of the tuning parameters is also shown in Figure 6(b). Similar to the linear case, in this problem, the tuning parameter β practically has a weak effect on the solutions. On the other hand, when no tuning parameter is applied, the solution is not only nonmonotonic but also the discontinuity is captured with wrong strength and position. As it is inferred from Figure 6(a), there is an expansion wave zone in the upstream and a constant state region in the down-stream of the front. It is well known that this problem appears when the entropy condition is not satisfied [7]. Also, it should be noticed that as the Rankine–Hugoniot condition is violated, the position of the wave front is not correct even though both of the tuning parameters are used. The solution of this problem, using the MSTEM algorithm is shown in Figure 7(a).

In order to study the effect of the residual saturations, another test case is studied in which the residual saturations of water and oil are 0.2. All other parameters remain the same as shown in Table I. The analytical solution can be found in Reference [7]. The numerical solution for this case, using the SSTEM algorithm is highly oscillatory and is not shown here. The numerical solution using the MSTEM algorithm is shown in Figure 7(b). In this

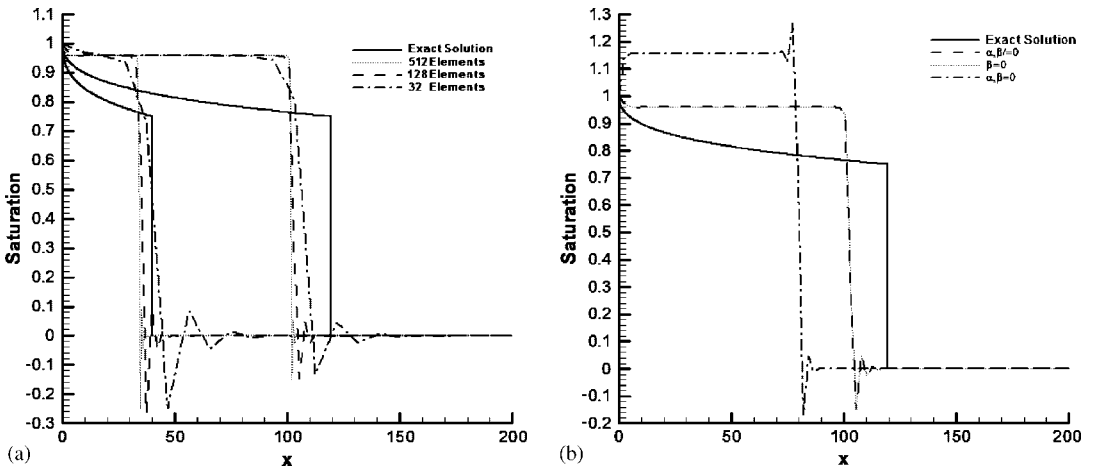

Figure 6. Case II—(a) comparison of results obtained on various grids using SSTEM algorithm with the exact solution; and (b) effect of tuning parameters on solution of the using SSTEM algorithm using 128 elements.

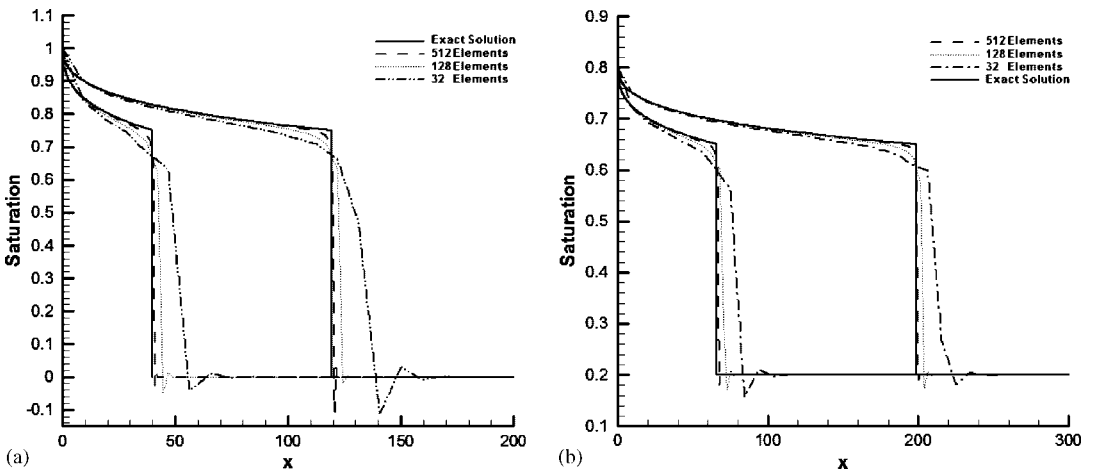

Figure 7. Case II—comparison of results obtained on various grids using MSTEM algorithm with the exact solution: (a) $S_{rw} = S_{rn} = 0$; and (b) $S_{rw} = S_{rn} = 0.2$.

case, the tangential saturation is 0.65 and the wave front after 1500 days reaches $x = 198.8$ m. As observed from the figure, the solution converges to the correct solution by increasing the number of elements.

In contrast to the numerical solution of the SSTEM algorithm, this solution satisfies both the Rankine–Hugoniot and Entropy conditions. It can be clearly seen that the scheme converges to the correct solution as the mesh is refined. Using the MSTEM algorithm the under-shoots in the downstream are always less than 10% while using the SSTEM algorithm produces large

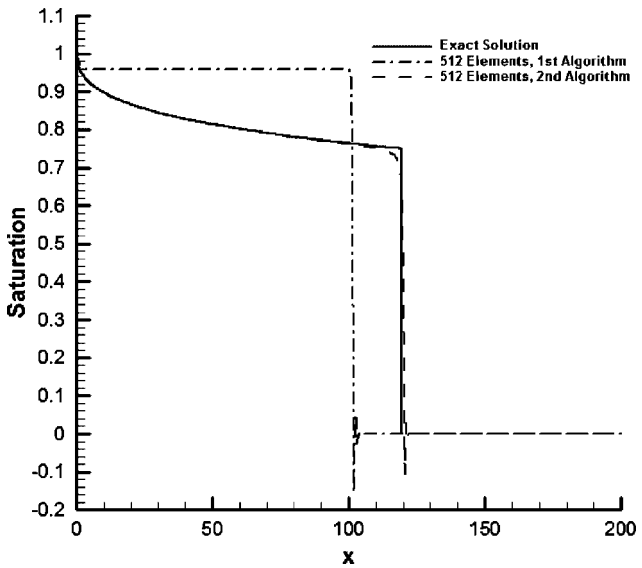

Figure 8. Case II—comparison of results obtained SSTEM and MSTEM algorithms.

under-shoots of up to 30% in the downstream. A comparison of the solutions obtained by these two algorithms is given in Figure 8. Although for the linear case the SSTEM algorithm behaves better than the MSTEM, the latter algorithm behaves much better for the nonlinear case.

5.3. One-dimensional case III: Brooks–Corey model for relative permeability with capillary pressure

In this test case, the effect of capillary pressure is taken into account. The problem is studied using both algorithms. Figures 9(a) and (b) show results of the SSTEM and MSTEM algorithms, respectively. In this case, the effect of tuning parameters is negligible. The computations show that both methods have the same accuracy and practically give identical solutions. From what was shown above, it can be deduced that in this case, the standard space–time Galerkin method can be used instead, producing the same accuracy.

5.4. Five-spot problem

It was seen from 1D test cases that the SSTEM cannot predict the position and strength of the saturation at the discontinuity. In the following 2D test cases, the MSTEM is used as the main method while the results of SSTEM are also shown for comparison. Linear quadrilateral elements are used throughout this study. Two of the computational grids used for this problem are displayed in Figure 10. The coarse grid has 768 elements and 825 nodes and the fine grid consists of 12 288 elements and 12 513 nodes. Here, three five-spot problems are solved to demonstrate the capability of the method in dealing with the 2D problems. These include one homogeneous and two heterogeneous problems. The physical domain has a constant porosity $\varepsilon = 0.2$. The residual saturations are $s_{\mathrm{rw}} = s_{\mathrm{rn}} = 0.2$. The initial pressure of the reservoir is

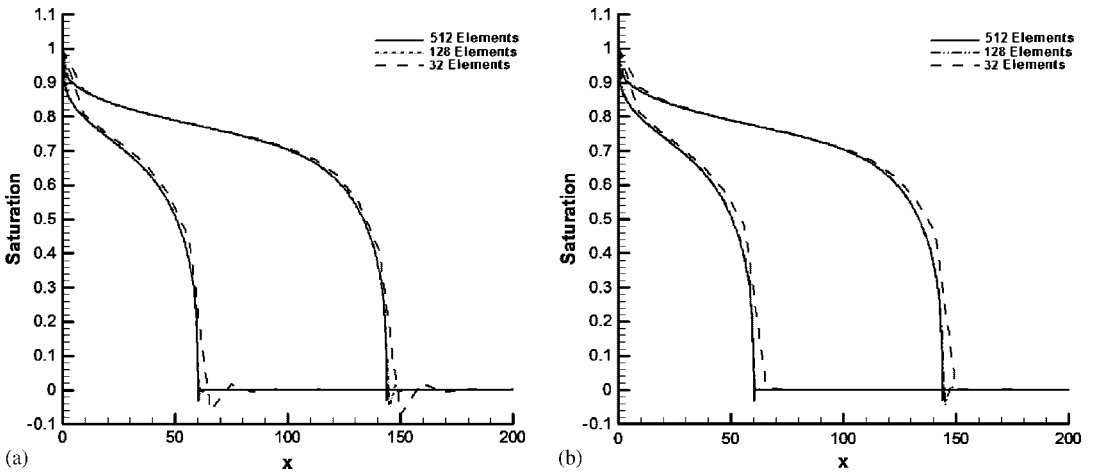

Figure 9. Case III—(a) results obtained by the SSTEM algorithm; and (b) the MSTEM algorithm for various grids.

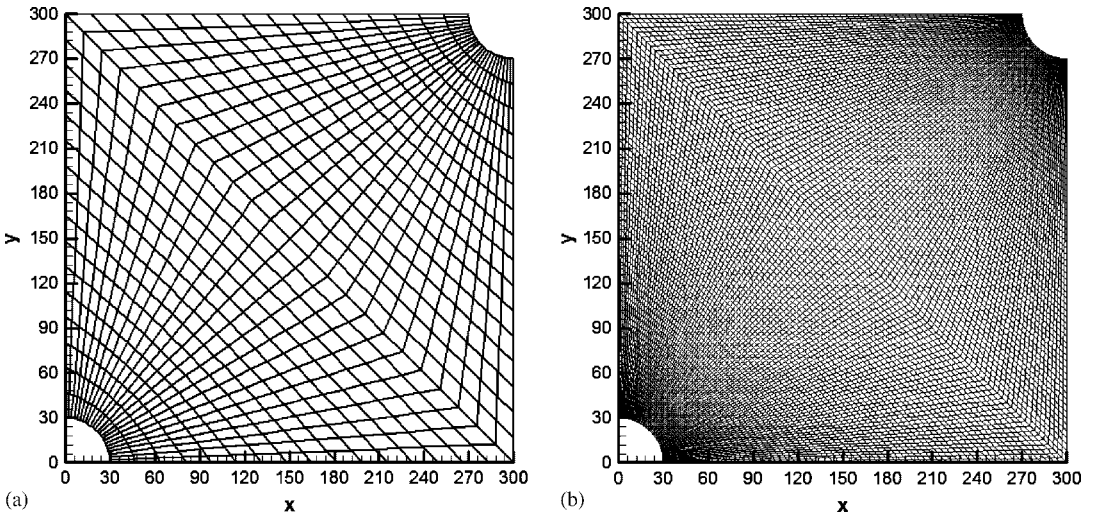

Figure 10. Typical computational grids used for the five-spot problems: (a) coarse; and (b) fine.

$P_{\text{init}} = 200\,\text{kPa}$. The Brooks–Corey model is used for the relative permeability functions. The water is injected from the lower left well and oil is produced from the upper right well. In all cases, the computational time step starts from one day and is adapted accordingly till the simulation period completes.

5.4.1. Case IV: homogeneous problem. In this problem, the absolute permeability is $K = 10^{-7}\,\text{m}^2$. The capillary pressure effect is negligible for this test case. The rate of water injection is 0.12 kg/s. In Figure 11, the contour plots of saturation distributions after 200 days obtained

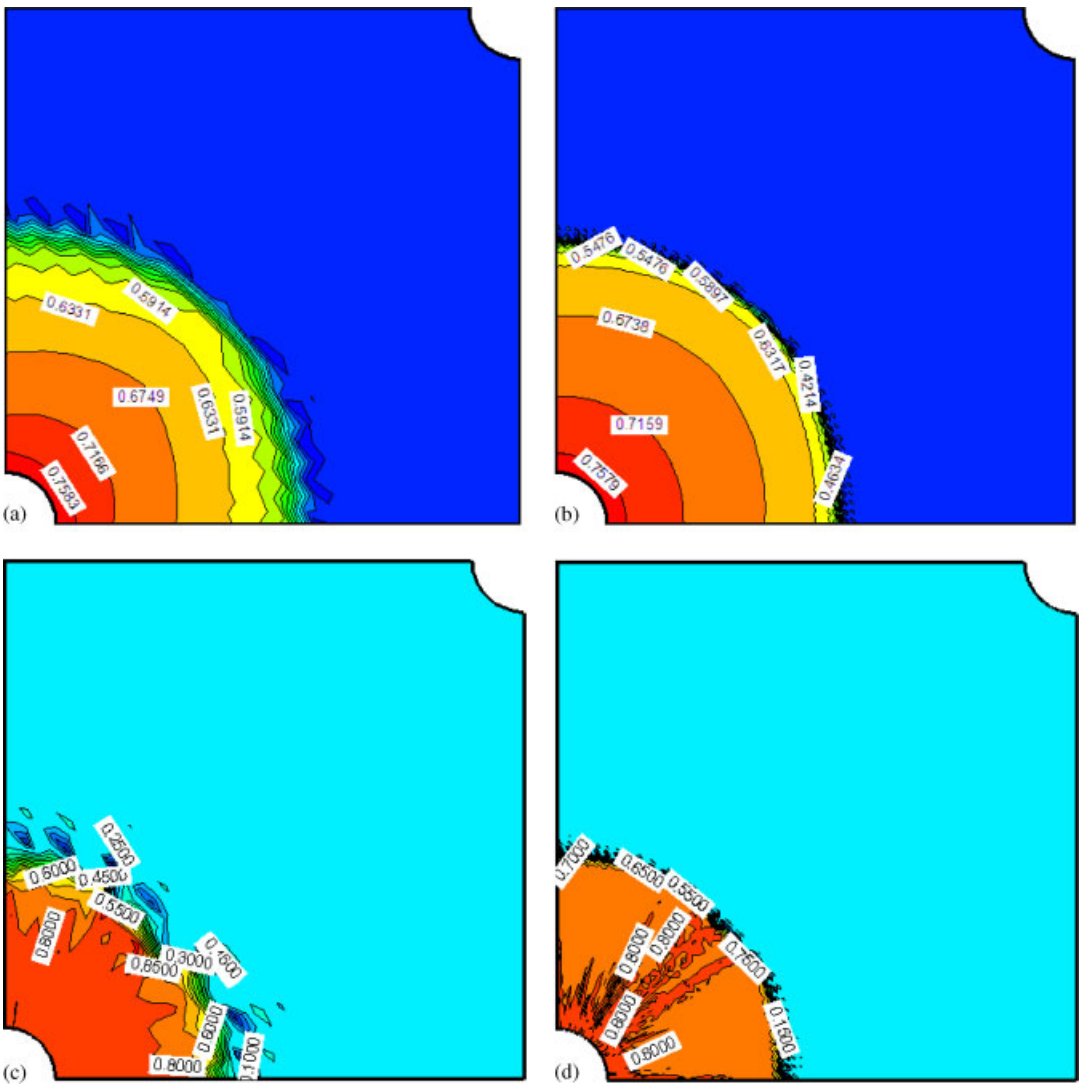

Figure 11. Case IV—contours of saturation obtained by the MSTEM on the: (a) coarse; (b) fine grids; contours of saturation obtained by the SSTEM on the: (c) coarse; and (d) fine grids.

by the SSTEM and MSTEM are compared for the coarse and fine grids. Figure 12 shows the streamlines and pressure contours obtained by MSTEM on the fine grid. In Figure 13(a) the cross-sectional saturation profiles obtained by the MSTEM are compared for different grids along the diagonal of the square. Also, Figure 13(b) compares the results obtained by the MSTEM and SSTEM methods along this diagonal. As it was seen in 1D cases, the solution obtained by the SSTEM shows an entirely wrong behaviour while the MSTEM demonstrates a significant improvement over the SSTEM.

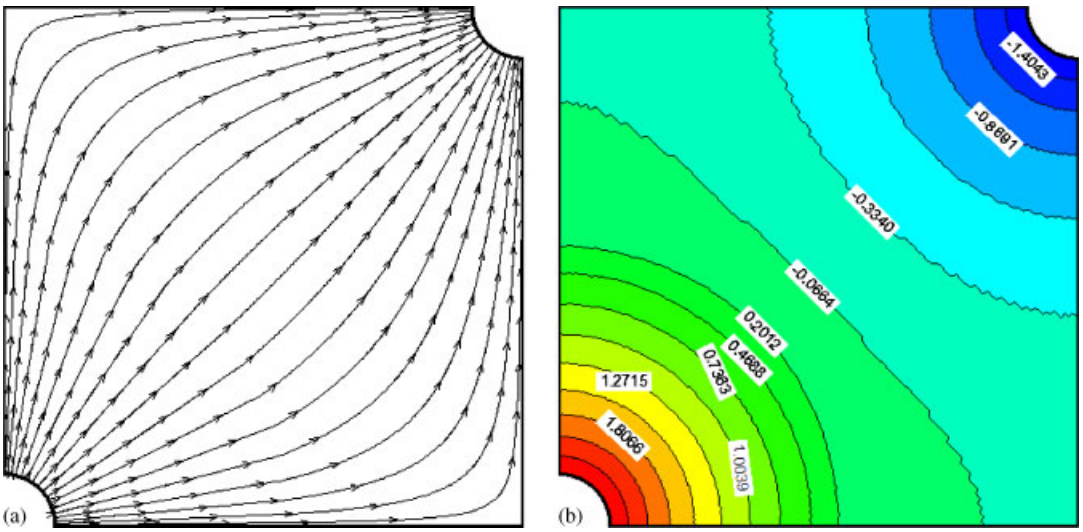

Figure 12. Case IV—(a) streamlines; and (b) pressure contours obtained on the fine grid.

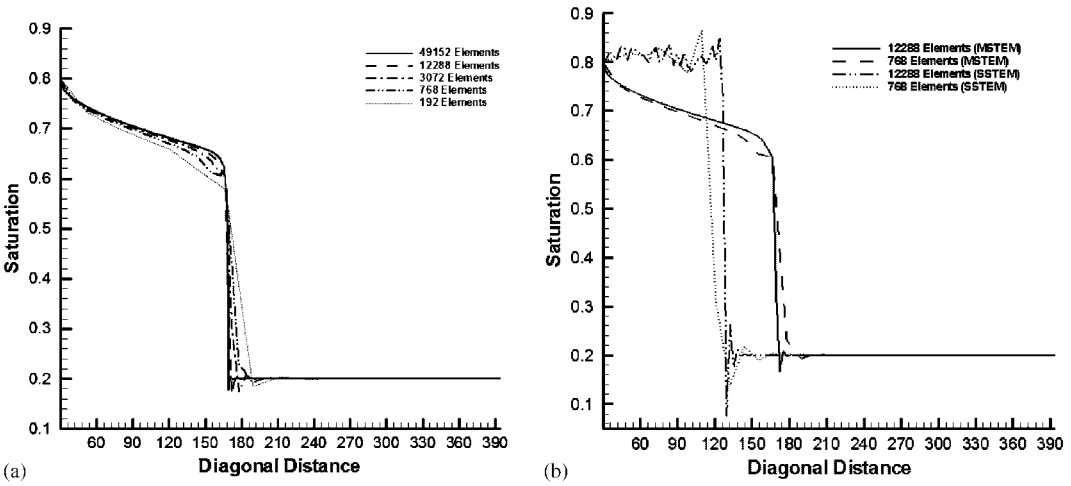

Figure 13. Case IV—(a) comparison of saturation distributions obtained by MSTEM across the diagonal for various grids; and (b) a comparison between MSTEM and SSTEM methods.

5.4.2. Case V: block heterogeneous problem. In this problem, the physical domain (Figure 14) consists of two permeable regions; the central core region has an absolute permeability $K = 10^{-10}\,\mathrm{m}^2$ and the surrounding background region has $K = 10^{-7}\,\mathrm{m}^2$. The rate of water injection is 0.12 kg/s. The contour plots of saturation distributions after 600 days are compared for the coarse and fine grids in Figure 15. The streamlines and pressure contours obtained on the fine grid are shown in Figure 16. Figure 17 shows the water front and 3D

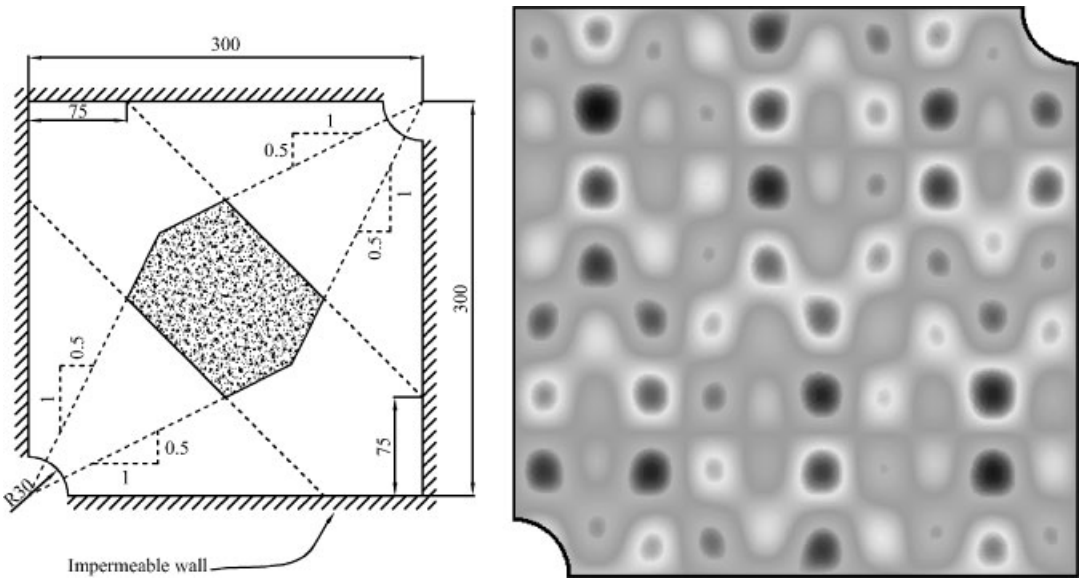

Figure 14. Physical domain and absolute permeability distributions for cases V and VI.

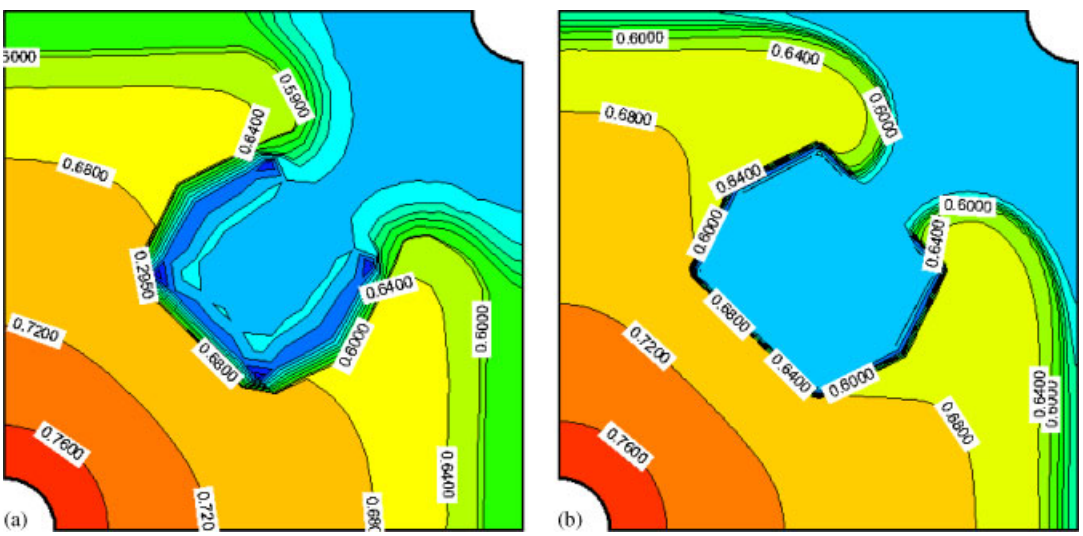

Figure 15. Case V—contours of saturation obtained on the: (a) coarse; and (b) fine grids.

representation of the pressure contours obtained using the fine grid. For this test case, no over-shoot is observed as long as the Peclet number is restricted to 20. The results prove that the modified method can properly handle discontinuities in the absolute permeability at the interfaces.

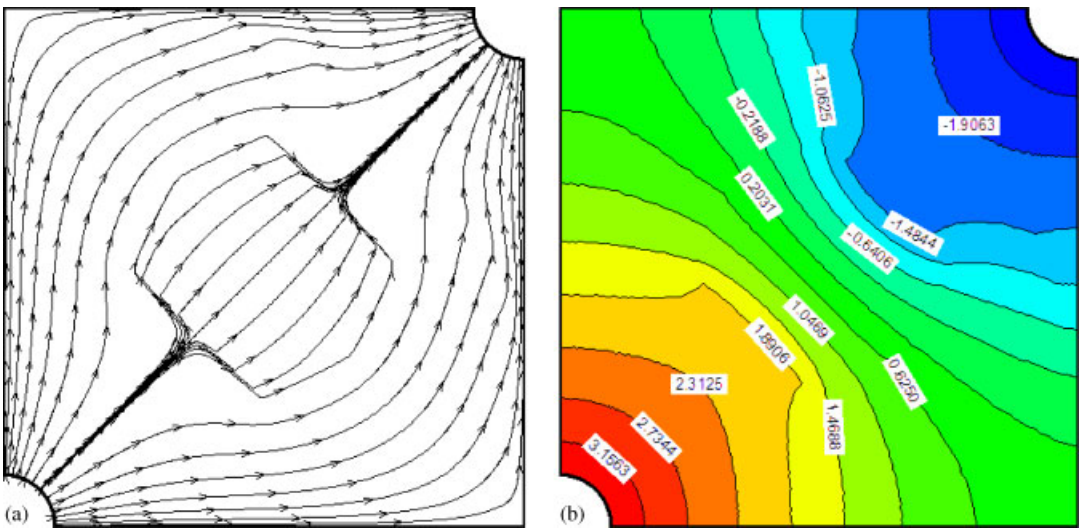

Figure 16. Case V—(a) streamlines; and (b) pressure contours obtained on the fine grid.

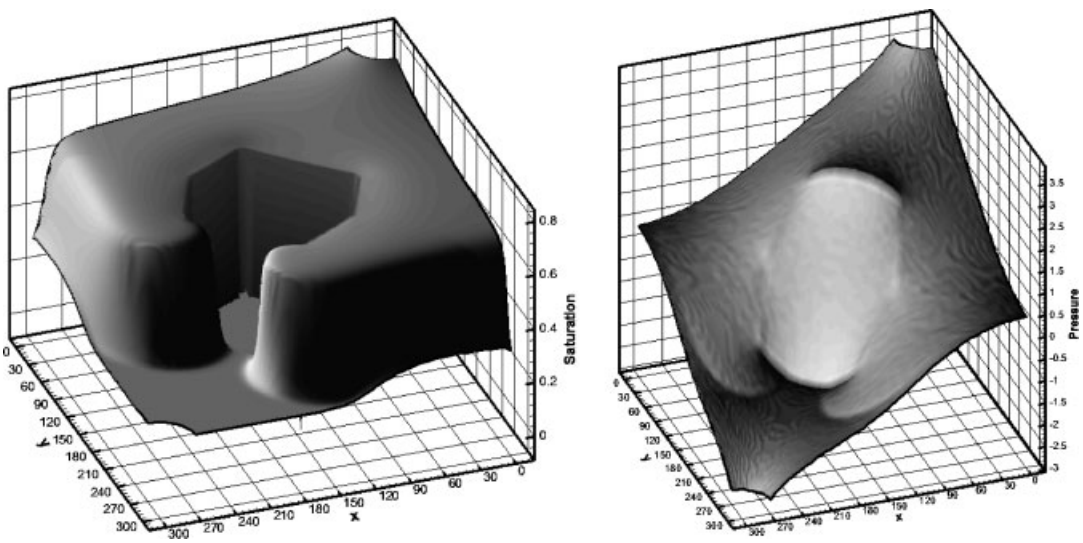

Figure 17. Case V—water front and pressure distribution after 600 days.

5.4.3. Case VI: continuous heterogeneous problem. In this problem, the physical domain consists of a region with a continuous absolute permeability defined by [29]

$$\log_{10} K = -7 + \sin(10\pi\bar{x})\sin(10\pi\bar{y}) + 0.7\sin(3\pi\bar{x})\cos(6\pi\bar{y}) + 0.3\sin(\pi\bar{x}/2)\sin(\pi\bar{y}) \quad (25)$$

where $\bar{x} = x/300$ and $\bar{y} = y/300$. The rate of water injection is 0.12 kg/s. The contour plots of saturation distributions after 600 days are compared for the coarse and fine grids in Figure 18.

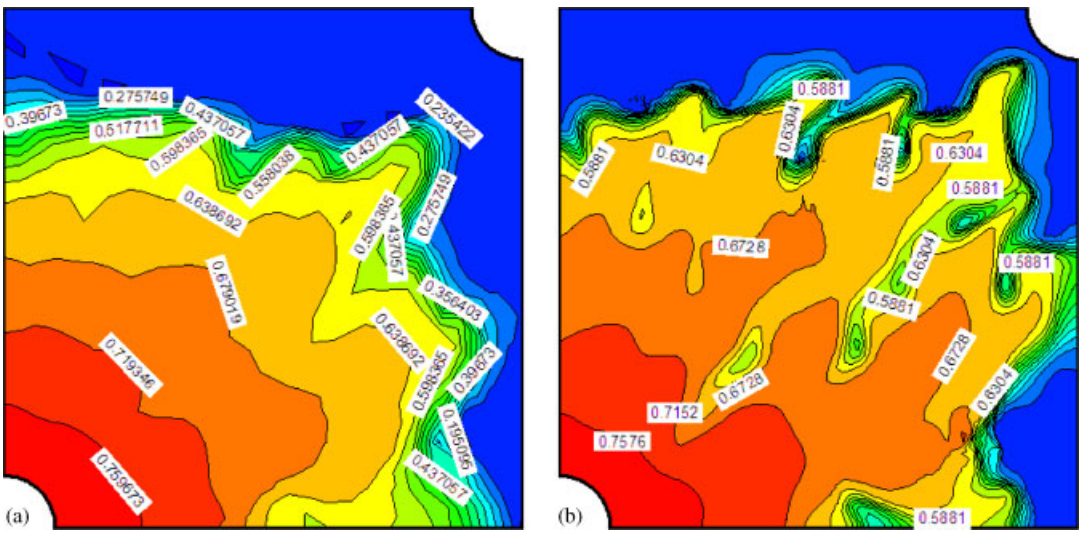

Figure 18. Case VI—contours of saturation obtained on the: (a) coarse; and (b) fine grids.

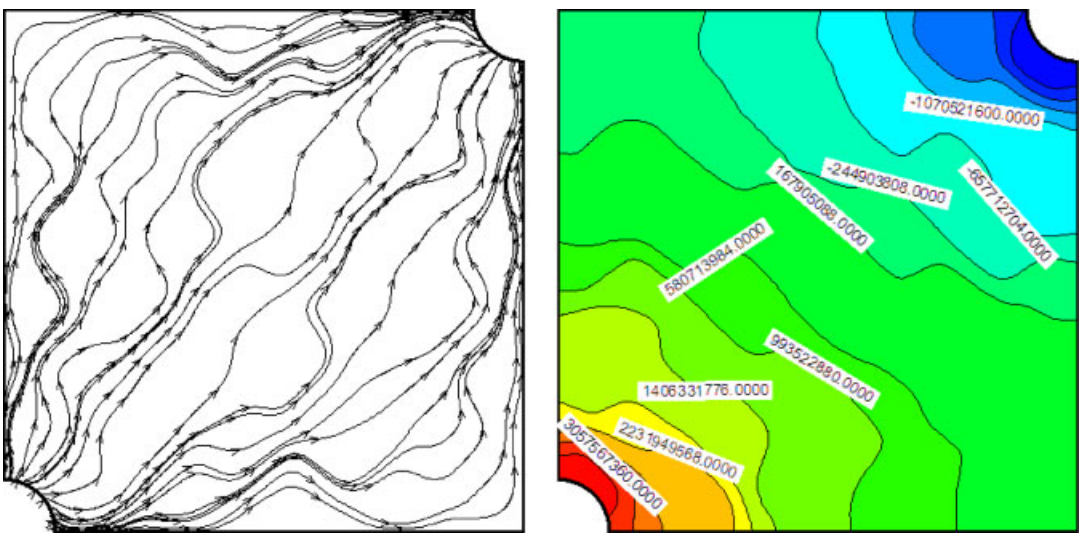

Figure 19. Case VI—streamlines (left) and pressure contours (right) obtained on the fine grid.

The streamlines and pressure contours obtained on the fine grid are shown in Figure 19. Figure 20 shows the water front and 3D representation of the pressure contours obtained using the fine grid.

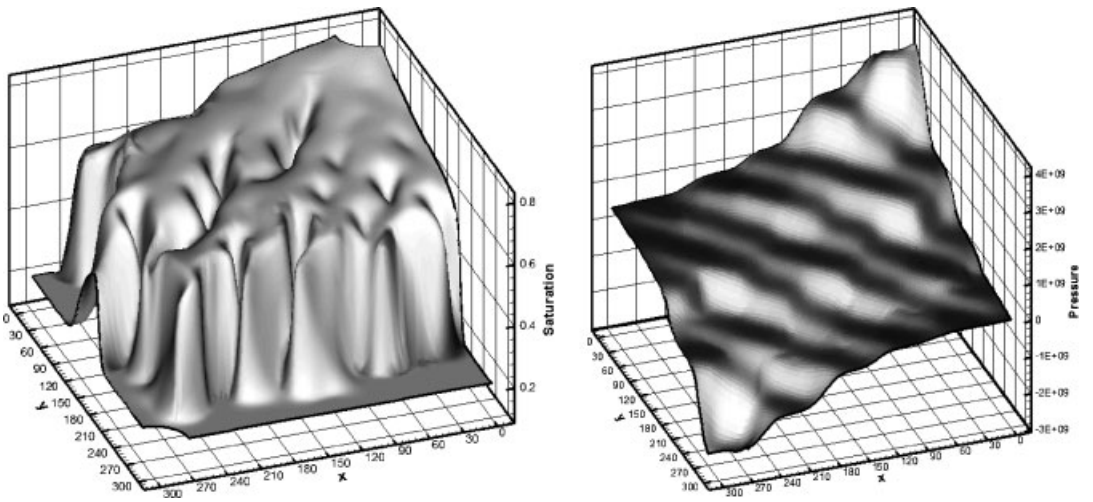

Figure 20. Case V—water front and pressure distribution after 600 days.

6. CONCLUSION

It was shown that the proposed modified space–time method performs well in comparison with the original Petrov–Galerkin space–time method. Although the modified method requires nearly double the amount of grid elements in discontinuous regions, for linear advection–diffusion problems with initial sharp discontinuities, it gives a monotone solution without noticeable phase error and over/under-shoots. It was also shown that for such problems tuning parameters do not have significant effect on the solution.

In nonlinear advection–diffusion problems, which are represented here by an immiscible two-phase flow in porous media, it was shown that while the original space–time method does not satisfy the Rankine–Hugoniot and the entropy conditions, the modified method does so by predicting the correct position and level of saturation at the wave front. The method exhibits some undershoots at the sharp front, which can be alleviated by limiting the solution in this region.

Numerical studies prove that the effect of capillary pressure helps the original method to achieve results as accurate as those obtained by the modified method. In other words, in low Peclet numbers, both algorithms give almost identical results. It can be concluded that for such problems extra diffusion and/or dispersion is required so that the standard Galerkin method can be used instead which can reduce the cost of solution.

Finally, it was shown that the modified method is extendible to 2D problems and can produce accurate results for homogeneous medium with discontinuous absolute permeability and heterogeneous media.

ACKNOWLEDGEMENTS

The support of this work by the Center of Excellence in Energy Conversion is gratefully appreciated. Authors also would like to thank Dr S. K. Hannani and Dr M. Razvan, for their very useful comments and invaluable discussions.

REFERENCES

1. Aziz K. Modeling of thermal oil recovery processes. In *Mathematical and Computational Methods in Seismic Exploration and Reservoir Modeling*, Fitzgibbon WE (ed.). SIAM: Philadelphia, PA, 1986; 3–17.
2. Aziz K, Settari A. *Petroleum Reservoir Simulation*. Elsevier: New York, 1986.
3. Lake LW. *Enhanced Oil Recovery*. Prentice-Hall: Englewood Cliffs, NJ, 1989.
4. Peaceman DW. *Fundamentals of Numerical Reservoir Simulation*. Elsevier: New York, 1989.
5. Sheorey T, Muralidhar K, Mukherjee PP. Numerical experiments in the simulation of enhanced oil recovery. *International Journal of Thermal Sciences* 2001; **400**(11):981–997.
6. Chavent G, Jaffre J. *Mathematical Models and Finite Elements for Reservoir Simulation*. Elsevier: Netherlands, 1986.
7. Helmig R. *Multiphase Flow and Transport Processes in the Subsurface*. Springer: Berlin, Heidelberg, 1997.
8. Chen Z, Ewing RE, Espedal MS. *Multiphase Flow Simulation with Various Boundary Condition in Computational Methods in Water Resources*, Peters A, Wittum G, Herrling B, Meissner U, Brebbia CA, Gray WG, Pinder GF (eds). Kluwer Academic Publishers: Netherlands, 1994; 925–932.
9. Ewing R. *The Mathematics of Reservoir Simulation*. SIAM: Philadelphia, PA, 1983.
10. Pao WKS, Lewis RW. Three-dimensional finite element simulation of three-phase flow in a deforming fissured reservoir. *Computer Methods in Applied Mechanics and Engineering* 2002; **191**:2631–2659.
11. Zienkiewicz OC, Taylor RL. *The Finite Element Method*, vol. 1 (5th edn). Butterworth-Heinemann: Stoneham, MA, 2000.
12. Morgan K, Peraire J. Unstructured grid finite-element methods for fluids. *Reports on Progress in Physics* 1998; **61**:569–638.
13. Chavent G, Cohen G, Jaffre J, Dupuy MPT, Ribera I. Simulation of two-dimensional water flooding by using mixed finite elements. *Society of Petroleum Engineers Journal* 1984; **24**(4):382–390.
14. Lewis RW, Schrefler BA. *The Finite Element Method in the Static and Dynamic Deformation and Consolidation of Porous Media* (2nd edn). Wiley: New York, 1998.
15. Masud A, Hughes TJR. A stabilized finite element method for Darcy flow. *Computer Methods in Applied Mechanics and Engineering* 2002; **191**:4341–4370.
16. Wheeler M, Yotov I. Mixed finite element methods for modeling flow and transport in porous media. *CRPC-TR95555-S*, Center of Research on Parallel Computation, Rice University, Houston, 1995.
17. Hughes TJR. *The Finite Element Method*. Prentice-Hall Inc.: Englewood Cliffs, NJ, 1987.
18. Heinrich JC, Pepper DW. *Intermediate Finite Element Method*: *Fluid Flow and Heat Transfer*. Taylor & Francis: New York, 1999.
19. Espedal M, Ewing RE. Characteristic Petrov–Galerkin subdomain methods for two-phase immiscible flow. *Computer Methods in Applied Mechanics and Engineering* 1987; **64**:113–135.
20. Cardle JA. A modification of the Petrov–Galerkin method for the transient convection–diffusion equation. *International Journal for Numerical Methods in Engineering* 1995; **38**:171–181.
21. Yu CC. Finite element analysis of time-dependent convection–diffusion equations. *Ph.D. Dissertation*, Department of Aerospace and Mechanical Engineering, University of Arizona, Tucson, 1986.
22. Yu CC, Heinrich JC. Petrov–Galerkin methods for the time-dependent convective transport equation. *International Journal for Numerical Methods in Engineering* 1986; **23**:883–901.
23. Hanshaw TC. A Petrov–Galerkin finite element solution to the time-dependent Burgers equation. *Master Thesis*, Department of Aerospace and Mechanical Engineering, University of Arizona, Tucson, 1981.
24. Huyakorn PS, Nilkuha K. Solution of transient transport equation using an upstream finite element scheme. *Applied Mathematical Modelling* 1979; **3**:7–17.
25. Saad Y. *Iterative Methods for Sparse Linear Systems*. PWS Publishing: Boston, 1996.
26. Hirsch C. *Numerical Computation of Internal and External Flows*, *Volume 2*: *Computational Methods for Inviscid and Viscous Flows*. Wiley: New York, 1988.
27. Leonard BP. The ultimate conservative differencing scheme applied to unsteady one-dimensional advection. *Computer Methods in Applied Mechanics and Engineering* 1991; **88**:17–74.
28. Lapidus A. A detached shock calculations by second order finite differences. *Journal of Computational Physics* 1967; **2**:154–177.
29. Riviere B, Bastian P. Discontinuous Galerkin methods for two-phase flow in porous media. *Technical Report 2004-28*. Kluwer Academic Publishers: Netherlands, 2004.

